Smart Structures and Systems, *Vol. 26, No. 4 (2020) 451-468*
DOI: https://doi.org/10.12989/sss.2020.26.4.451

Finite element model updating of a cable-stayed bridge using metaheuristic algorithms combined with Morris method for sensitivity analysis

Long V. Ho[1,2a], Samir Khatir[1b], Guido D. Roeck[4], Thanh Bui-Tien[3] and Magd Abdel Wahab*[5,6]

[1]Faculty of Engineering and Architecture, Ghent University, Technologiepark Zwijnaarde 903, B-9052 Zwijnaarde, Belgium
[2]Faculty of Civil Engineering, University of Transport and Communications, Campus in Ho Chi Minh, 450-451 Le Van Viet, District 9, Ho Chi Minh, Vietnam
[3]Faculty of Civil Engineering, University of Transport and Communications, 03 Cau Giay, Dong Da District, Ha Noi, Vietnam
[4]Department of Civil Engineering, KU Leuven, B-3001 Leuven, Belgium
[5]Division of Computational Mechanics, Ton Duc Thang University, Ho Chi Minh, 19 Nguyen Huu Tho, District 7, Ho Chi Minh, Vietnam
[6]Faculty of Civil Engineering, Ton Duc Thang University, Ho Chi Minh, 19 Nguyen Huu Tho, District 7, Ho Chi Minh, Vietnam

(*Received November 19, 2019, Revised July 7, 2020, Accepted July 8, 2020*)

Abstract. Although model updating has been widely applied using a specific optimization algorithm with a single objective function using frequencies, mode shapes or frequency response functions, there are few studies that investigate hybrid optimization algorithms for real structures. Many of them did not take into account the sensitivity of the updating parameters to the model outputs. Therefore, in this paper, optimization algorithms and sensitivity analysis are applied for model updating of a real cable-stayed bridge, i.e., the Kien bridge in Vietnam, based on experimental data. First, a global sensitivity analysis using Morris method is employed to find out the most sensitive parameters among twenty surveyed parameters based on the outputs of a Finite Element (FE) model. Then, an objective function related to the differences between frequencies, and mode shapes by means of MAC, COMAC and eCOMAC indices, is introduced. Three metaheuristic algorithms, namely Gravitational Search Algorithm (GSA), Particle Swarm Optimization algorithm (PSO) and hybrid PSOGSA algorithm, are applied to minimize the difference between simulation and experimental results. A laboratory pipe and Kien bridge are used to validate the proposed approach. Efficiency and reliability of the proposed algorithms are investigated by comparing their convergence rate, computational time, errors in frequencies and mode shapes with experimental data. From the results, PSO and PSOGSA show good performance and are suitable for complex and time-consuming analysis such as model updating of a real cable-stayed bridge. Meanwhile, GSA shows a slow convergence for the same number of population and iterations as PSO and PSOGSA.

Keywords: Kien bridge; PSO; GSA; PSOGSA; global sensitivity analysis

1. Introduction

The application range of vibration-based monitoring is very broad. It focuses not only on defect detection, but also is used to inspect and control construction quality, model calibration and verification of design factors, providing a stop warning for traffic, proposing maintenance plans and predicting serviceability of structures. Depending on the followed approach, a large number of sensors or a few sensors combined with a numerical model are needed (Peeters 2000). A benchmark or baseline FE model needs to be generated by using dynamic properties from experiments. However, a mismatch always exists between the FE model based on as-built documents and experimental results due to various uncertainty sources. These sources can be due to (i) modelling of physical uncertainties, e.g., boundary conditions, geometric dimensions, material properties, etc., (ii) numerical uncertainties, i.e., element types, mesh size, human mistakes, etc. and (iii) measurement errors, e.g., unsuitable sensor, noise, synchronization and data processing errors, etc. Therefore, after reducing uncertainties in simulation and testing, model parameters have to be updated in order to decrease the mismatch. Generally speaking, there are two types of model updating methods, namely direct methods and iterative methods. The dominant advantage of direct methods is computational efficiency because the system mass and stiffness matrices are directly updated (Carvalho *et al*. 2007, Cottin and Reetz 2006). However, the obtained matrices may have no physical meaning and cannot be suitable for engineering judgment. The iterative methods minimize the differences between numerical and experimental results by updating values of the most sensitivity parameters to the model outputs in an iterative process. The latter provides flexible choices for updating parameters that are utilized within an objective function. The efficiency of model updating can be improved when it is combined with optimization algorithms. Numerous researchers successfully applied several optimization techniques such as Genetic Algorithms (GA) and Particle Swarm Optimization (PSO) by Tran-Ngoc *et al*. (2018), improved PSO for a cable-

*Corresponding author, Professor,
E-mail: magd.abdelwahab@tdtu.edu.vn
[a] Student, E-mail: HoViet.Long@Ugent.be
[b] Ph.D., E-mail: Khatir_samir@hotmail.fr

http://www.techno-press.org/?journal=sss&subpage=7   ISSN: 1738-1584 (Print), 1738-1991 (Online)

stayed bridge by Hoa *et al*. (2020) and PSO combined with orthogonal diagonalization for a truss bridge by Tran-Ngoc *et al.* (2020). Some authors combined them with a surrogate model, e.g., Kriging model by Qin *et al.* (2018) or response surface method by Deng and Cai (2010), Islam *et al.* (2018) and Ghiasi and Ghasemi (2018) to reduce the computational cost. A few studies utilized hybrid optimization for updating model parameters. Recently, some new optimization algorithms and their hybrid forms are proposed, namely Gravitational Search Algorithms (GSA) and combined PSOGSA. These algorithms demonstrated their validity for mathematical optimization problems thanks to cheap cost and accuracy compared with previous algorithms (Rashedi *et al*. 2009, Mirjalili *et al.* 2014). Khatir *et al.* (2018) used Particle Swarm Optimization (PSO) to calibrate the FE model of beam-like structures using experimentally measured natural frequencies. A comparison between Isogeometric Analysis (IGA) and Finite Element Method (FEM) based on measurements is considered by Khatir *et al*. (2019). A model updating based on Teaching-Learning-Based Optimization Algorithm (TLBO) was presented by including vertical springs. More accurate results were obtained based on experimental data. Khatir *et al.* (2019) presented an application for model updating using Cuckoo Search algorithm (CS) based on measured data. The parameters considered for this application were the IGA parameters, which were based on NURBS order and discretization in two-dimensional space. Furthermore, Khatir *et al.* (2020) also applied a hybrid TLBO-PSO-ANN for fast damage identification in steel beam structures using IGA. A novel meta-heuristic optimization algorithm, namely Balancing Composite Motions (BCMO) was developed by Le-Duc *et al*. (2020). It is worth mentioning that no algorithm-specific parameter is required in constructing the algorithm. Therefore, the implementation of BCMO is easy and simple for solving varieties of optimization problem. The application of BCMO in several benchmark problems and especially in three real engineering design problems, proved its effectiveness and robustness. Besides the traditional model updating method based on FEM, it becomes very interesting when artificial neural networks and adaptive collocation strategy for an inverse acoustics problem are used (Anitescu *et al.* 2019). The obtained results with good accuracy proved that this method could be successfully applied for stochastic analysis, for both forward and inverse problems. However, the application of these algorithms on bridge structures is uncommon. Hence, it is necessary to investigate the application of these optimization techniques for real structures. Some popular objective functions that are often widely used, make use of natural frequencies, mode shapes by mean of MAC index and frequency response functions (Lin and Ewins 1994). In this paper, another direct usage of mode shape, COMAC or enhanced COMAC (known as eCOMAC), is investigated. The obtained results are compared with those obtained by more traditional objective functions.

Besides that, in model updating, choosing the right updating parameters from the FE model is extremely important. Sometimes, this depends on experience of engineers or based on engineering judgment (Altunisik and Alemdar 2017). Updating parameter selection is not an easy task, especially in complex structures because of the uncertainties in boundary conditions, real values of material properties, variances of geometric dimensions, etc. A good selection not only achieves a superior match between experimental and numerical data, but also reduces significantly the computational time. Hence, it is necessary to use a reliable sensitivity measure to identify updating parameters among various uncertainties. One of the common purposes of sensitivity analysis is to determine the most influential factors on the outputs. In other words, sensitivity analysis helps engineers to have a comprehensive view about input-output relationship. In general, sensitivity analysis can be classified by several specifications. For instance, based on the manner of variation of parameters, global sensitivity analysis, and local sensitivity analysis are defined. In comparison with local sensitivity analysis, the global sensitivity analysis methods are independent of linearity of relationship between inputs and outcomes. Consequently, a wide applicability is the advantage of these methods. Sobol and Morris' method can be referred to as global sensitivity analysis. Sobol (2001) developed a new global sensitivity analysis approach by utilizing Monte Carlo based integration to estimate the impact of every single input parameter, as well as all input parameters on model results. The first index is the first-order effect sensitivity index. This index reveals the effect of individual inputs on the change in model outputs. The second index is the total effect sensitivity index, which measures the shift of outputs due to the interaction between inputs. Many subsequent studies used Sobol method effectively. Wan and Ren (2015) combined Gaussian process meta-model and Sobol approach to identify important parameters in a steel plate and in a real arch bridge. The obtained results revealed the reliability and feasibility of the proposed approach. However, in order to achieve an affordable accuracy of sensitivity indices, authors used a high number of sample size N for Monte Carlo discretization. It means that this method is very time-consuming. The number of required simulation runs is calculated as $t = N \times 2 \times (p + 1)$ with p is number of input parameters. There is another common method for sensitivity analysis, namely Morris method also known as Element Effects (EE) method. In EE method, the effect of each input is calculated by dividing the variance of output by variance of one input. The method, which was derived from one at a time method, was developed by Morris (1991). According to the obtained sample points from a good trajectory, the calculation of a group of EEs is a good step to achieve a global result. In this method, two indices are determined for ranking model parameters based on the output. The first factor is the mean value, μ, which represents the level of influence of an input on the model output. The second factor is the standard deviation, σ, which represents the level of independence of an input's influence on other inputs. The number of required runs for model evaluation of this method is $t = r \times (p + 1)$, where the number of parameters is p and the number of trajectories is r. Campolongo *et al.* (2007) proposed a modified mean

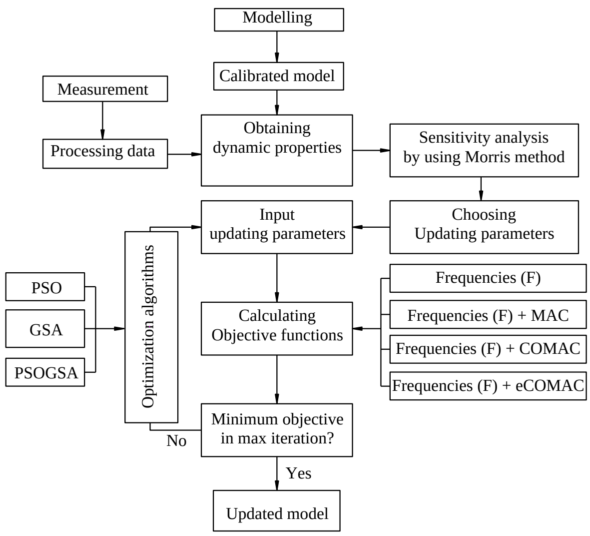

Fig. 1 Methodology flowchart

index, μ*, with absolute values of EEs to overcome the limitation of a monotonic model. Updating parameters of a heritage structure was chosen by Boscato *et al.* (2015) using Morris method. The obtained results confirmed the validity and reliability of the method. Menberg *et al*. (2016) conducted a comparative study on computational costs and extractable information between Morris method, linear regression analysis and Sobol method. It was found that the computational cost of Morris method was much lower than that of Sobol method. A combination of Morris method and Sobol index was carried out and applied to a composite beam by Feng *et al.* (2019). They only used the modified mean index μ* for comparison purpose with their proposed index because of its reality. A toolbox for uncertainty and sensitivity analysis methods was developed by Vu-Bac *et al*. (2016). In this toolbox, the authors combined three components: sampling methods of input parameters, surrogate model, and implementing Sobol's method for sensitivity analysis. The study was applied successfully to computationally expensive models. Hamdia *et al.* (2017) proposed a methodology for stochastic analysis of the fracture in polymer nanocomposites. Based on sensitivity analysis using Sobol' method, they constructed a polynomial chaos expansion surrogate model of six input parameters. The two significant parameters, the maximum allowable principal stress and Young's modulus of the epoxy matrix, were determined from the obtained results. A comparison study of sensitivity and uncertainty analysis for a pure flexoelectric beam and a composite beam was conducted by Hamdia *et al.* (2018). In this study, the authors used three sensitivity analysis methods, namely Morris One-at-a-time, PCE-Sobol' and extended Fourier amplitude sensitivity test. From the results, they not only indicated the most dominant parameters, but also showed the significant interaction effects of the material properties. For a practical and complex structure as the surveyed Kien bridge, computational costs should be considered. Therefore, in this paper, Morris method is employed for sensitivity analysis and μ* index is used to rank the model factors based on their importance.

A metaheuristic algorithm is applied to build a baseline model for the Kien bridge. The proposed approach consists of two successive steps. In the first step, a global sensitivity analysis method is used to identify the important parameters for the model outputs. In the second step, the reliability and effectiveness of three optimization algorithms are investigated by mean of objective functions. Dynamic responses of the benchmark model are compared with the real behaviour of the bridge. The methodology followed in this paper is illustrated by the flowchart shown in Fig. 1.

2. Morris screening method for sensitivity analysis

The more uncertain input parameters in the FE model, the more uncertain output parameters are. Therefore, in order to increase credibility, as well as, accuracy of numerical results, Morris method for sensitivity analysis is indispensable. Some parameters should be chosen before conducting the sensitivity analysis process. The value of sampling step, Δ, for each input parameter should remain the same between [0-1] regardless the different magnitudes of individual inputs. The choice of Δ is related to the number of levels p, i.e., $\Delta = p/[2 \times (p - 1)]$ with p an even value. However, the choice of p is dependent on the choice of sampling size r. Many previous studies found that values of $p = 4$ and $r = 10$ can create superior results. In his experiments, Morris used $r = 4$, a minimum value that could generate reliable results (Saltelli 2004). Hence, when $p = 4$ and $\Delta = 2/3$, the selection probability of each level (0, 1/3, 2/3, 1) is similar. Assuming that with the number of variables is k, in order to calculate k element effects, an input space $(k + 1)$ by r or $(k + 1) \times r$ sample points should be constructed.

The method begins with a set $X = \{0, 1/(p - 1), 2/(p - 1), \ldots, 1\}$. Then a random starting points x* is chosen from space X. These points x* are used to form other sampling points, i.e., x_i^j, $i \in (1, 2, \ldots, k)$ and $j \in (1, 2, \ldots, k + 1)$ by adding randomly Δ to at least one component of x*. The trajectory is closed until all sampling points x^{k+1} are generated. Note that the difference between two successive sampling points is only located in one component j^{th} of a trajectory. After evaluating the model at all points in each trajectory, the EE for each input variable k is calculated as

$$EE_i^l = \frac{f(x_i + \Delta) - f(x_i)}{\Delta} \text{ if } \Delta \text{ is an increase value of } x_i \quad (1)$$

$$EE_i^l = \frac{f(x_i) - f(x_i + \Delta)}{\Delta} \text{ if } \Delta \text{ is a decrease value of } x_i \quad (2)$$

where $f(x_i + \Delta)$ and $f(x_i)$ are corresponding outputs of input variables $(x_i + \Delta)$ and (x_i), respectively.

Modified mean index, μ_i^*, for assessing the overall effect of an input on output of i^{th} variable through r trajectory can be estimated as

$$\mu_i^* = \frac{\sum_{l=1}^{r} \left| EE_i^l \right|}{r} \quad (3)$$

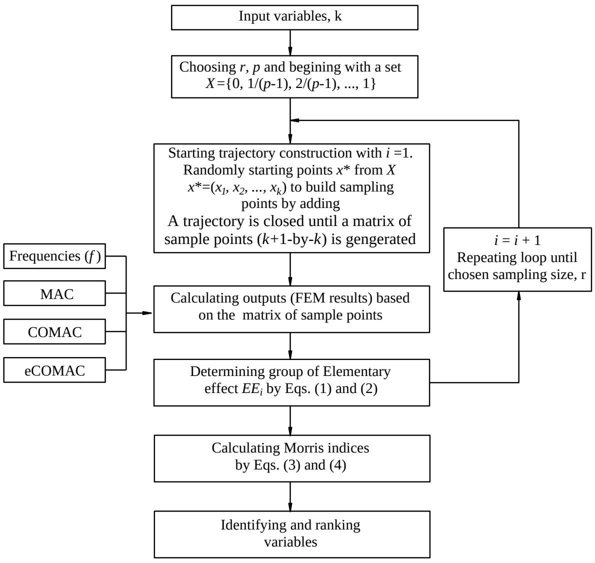

Fig. 2 Step-by-step Morris method

Standard deviation index δ, for estimating the interaction with other inputs is calculated as

$$\delta_i = \sqrt{\frac{1}{r}\sum_{l=1}^{r}(EE_i^l - \mu_i^*)^2} \tag{4}$$

The implementation of Morris method is shown in Fig. 2. For details of the implementation procedure of the method, the interested reader may consult Saltelli (2004).

3. Theory of metaheuristic algorithms

3.1 Particle swarm optimization algorithm (PSO)

The starting point of PSO is derived from natural social behaviour as well as dynamic moving of birds, fish or insects. Kennedy and Eberhart (1995) proposed an evolutionary technique for optimization problems. Self-experiences and social experiences are combined in the technique. To look for the best solution (or the best particle), a swarm movement (or flying) is generated around multi-dimensional search space (possible solutions) by using a number of particles (or candidate solutions). During the process of evolution, particle's experience is accumulated with shifted position, speed, and move forward to promising space to achieve the global maximum (or minimum). It means that each particle (or agent) self-regulates its moving based on its self-experience with regard to other particles' experience. By mean of updating the current position, as well as, current velocity after each iteration, the personal best of each particle (*pbest*) and the global best of all particles (*gbest*) are obtained. Dominant advantages of PSO are its simple programmability and quite low computational cost. Mathematic equations of PSO or particle update rules for velocity and position of each particle are as follows

$$v_i(t+1) = \omega \times v_i(t) + c_c \times rand_{(0\text{-}1)} \times [pbest_i(t) - x_i(t)] + c_s \times rand_{(0\text{-}1)} \times [gbest_i(t) - x_i(t)] \tag{5}$$

$$x_i(t+1) = x_i(t) + v_i(t+1) \tag{6}$$

where, $v_i(t+1)$ is velocity of particle i at iteration $(t+1)$, which can be identified based on exploration ability $\omega \times v_i(t)$, particle's memory $c_c \times rand_{(0\text{-}1)} \times [pbest_i(t) - x_i(t)]$ and collaboration of particles $c_s \times rand_{(0\text{-}1)} \times [gbest_i(t) - x_i(t)]$. The first part keeps each particle flying in the same original direction. The second part returns to the particle's personal best position in the search space. The last part causes particle to fly to the global best in the multi-dimension search space. The value of the inertial coefficient ω varies often from 0.8 to 1.2. The cognitive coefficient c_c and the social coefficient c_s lie between [0-2], but close to 2. Random values $rand_{(0\text{-}1)}$ are uniformly distributed in a range of [0-1]. Firstly, PSO is kicked off by a random set of particles' positions in search the region. The velocity of each particle is calculated in every single iteration. Then positions of particles are identified based on their updated velocities. After identifying the updated positions of particles, fitness of each particle relevant to the objective function is calculated. The changing process of particles' position continues until termination criteria is met (max iteration or small deviation between two successive values of objective function).

3.2 Gravitational search algorithm (GSA)

In 2009, inspired by the Newton law of gravity as well as mass interactions between agents in universe, Rashedi *et al*. (2009) developed a new heuristic optimization method, namely Gravitational Search Algorithm (GSA). Gravity force causes agents to interact with the other according to their mass. Following Newton law, the gravity causes a lighter mass to move towards heavier mass. In other words, the heavier the agent, the slower its motion and the larger gravity force. The heaviest agent can be considered as representative of the global optimum value or the best optimal solution. According to the law of gravity, at a specific time t, with a Euclidian distance $R_{ij}(t)$ between two agents and their random positions $x_j(t)$, $x_i(t)$ in search space, ε is a small constant, the attraction force applied on agent i from agent j can be identified as

$$F_{ij}(t) = G(t) \times \frac{M_{pi}(t) \times M_{ai}(t)}{R_{ij}(t)+\varepsilon} \times \left(x_j(t) - x_i(t)\right) \tag{7}$$

where

$$R_{ij}(t) + \varepsilon \approx norm\left(x_j(t) - x_i(t)\right) \tag{8}$$

where M_{pi} and M_{aj} are a passive and active gravitational mass of i and j agents, respectively. Mass of agent i is determined using the best, worst and current values of fitness

$$M_i(t) = \frac{m_i(t)}{\sum_{j=1}^{N} m_j(t)} \tag{9}$$

$$m_i(t) = \frac{fitness_i(t) - worst(t)}{best(t) - worst(t)} \tag{10}$$

The gravitational constant $G(t)$ at time t is calculated based on an initial value G_0 and reducing coefficient α as

$$G(t) = G_0 \times e^{\left(-\alpha \frac{\text{current} - \text{iteration}}{\text{max} - \text{iteration}}\right)} \tag{11}$$

Assuming that with N agents (masses) in a system, the total gravitational force on agent i, is calculated using a random sum of components of forces from other agents with the condition $j \neq i$

$$F_i(t) = \sum_{j=1, j \neq i}^{N} rand \times F_{ij}(t) \tag{12}$$

According to the law of motion, when gravity force is applied to agent, it moves with acceleration according to the magnitude of force and mass of agent. Therefore, the acceleration of agent i, at time t is given by

$$a_i(t) = \frac{F_i(t)}{M_i(t)} \tag{13}$$

Same as for PSO, during the search process, each agent updates its velocity and position until an end criterion is met. The new velocity of the agent is identified by the current velocity and acceleration. Similarly, the next position is calculated using the current position and the next velocity

$$v_i(t+1) = rand \times v_i(t) + a_i(t) \tag{14}$$

$$x_i(t+1) = x_i(t) + v_i(t+1) \tag{15}$$

3.3 Hybrid optimization algorithm PSOGSA

From the idea of a co-evolutionary algorithm, Mirjalili *et al*. (2014) proposed a new hybrid PSOGSA, combining two algorithms PSO and GSA. In this hybrid algorithm, both algorithms PSO and GSA run simultaneously to find out the best solution. Therefore, social thinking and local search ability in PSO and GSA, respectively, are associated. The foundation of PSOGSA relies on GSA. It starts with the calculation of gravitational forces, then acceleration of agents (particles). After identifying the best fitness so far in every iteration, Mirjalili *et al*. (2014) updated velocities of agents (particles) using the following equation

$$\begin{aligned} v_i(t+1) &= \omega \times v_i(t) + c_c \times rand_{(0\text{-}1)} \times a_i(t) \\ &+ c_s \times rand_{(0\text{-}1)} \times [gbest_i(t) - x_i(t)] \end{aligned} \tag{16}$$

In the above equation, the acceleration of agent (particle) i at time t, $a_i(t)$ is used to replace $[pbest_i(t) - x_i(t)]$ in Eq. (5), while other parameters remain the same. Then, agent's (particle's) positions are calculated after each iteration using the same equation as PSO and GSA

$$x_i(t+1) = x_i(t) + v_i(t+1) \tag{17}$$

Fig. 3 General view of Kien cable stayed bridge

The update of velocity and position of all agents (particles) is stopped when the termination condition is satisfied.

4. Measurements on Kien bridge

4.1 Introuction to Kien bridge

In the framework of the VLIR-UOS research project VN2018TEA479A103, the vibration measurement campaign of Kien bridge was carried out in November 2018. Kien bridge carries a two-lane traffic road (No. 10 Highway) and two lanes for both pedestrians and cyclists over the Cam river in Vietnam. The main structure system is a cable-stayed bridge with a 3-span continuous pre-stressed concrete box girder spanning over 85 m + 200 m + 85 m. The main cable-stayed bridge was constructed by using a balanced cantilever method from 2001 to 2003 in a Vietnam-Japan joint project. The approach bridge consists of 12 simply supported pre-stressed concrete spans, each of which has 34 meters (see Fig. 3). The entire width of the bridge is 16.7 m for the main bridge and 15.1 m for the approach bridge. The cross-section of the main bridge is a 3-cell box girder with a constant height of 2.2 m, while the approach bridge consists of six pre-stressed concrete I-beams.

The bridge includes two cable planes, which are 17.6 m far from each other. The height of the H-pylon with a solid rectangle cross-section is 51.5 m from the deck and 59.5 m from the top of the pile cap. From these pylons, 72 cables are stretched down diagonally to both sides and support the box girder. The stay cables in Kien bridge are arranged in a fan configuration. The inclined angle of the cable ranges from 30.44° to 50.37°. The length of stay cables varies from 20 m at the pylon to 103 m at mid-span and 95 m at the approach piers. A tendon consists of 37 to 48 strands of 15.2 mm diameter. Quality of strand satisfies the requirements of AASHTO M203 (ASTM416M). The stay cable was stressed using strand-by-strand cable installation with the allowance tensile stress of 0.55 f_{pu} during construction.

The objectives of measurements are: (i) to identify the modal parameters of the bridge under ambient load and (ii) to achieve a suitable numerical model as a baseline model for further study and future structural health monitoring activities.

4.2 On-site measurement campaign

Based on the obtained results from the initial FE model,

(a) Recording time response

(b) Sensor placement

Fig. 4 Instrumentation for data acquisition in the field

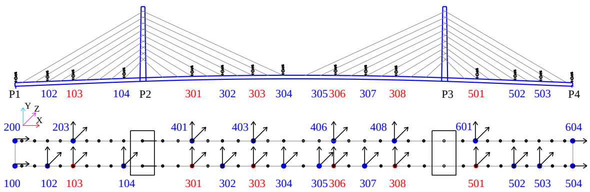

Fig. 5 Placement of measurement points on Kien bridge (red: reference nodes, blue: roving nodes, ↑: transversal, ↗: vertical, →: longitudinal)

a measurement plan was set up. Excitation, instrumentation, measurement setups, and data acquisition are presented in this section (Fig. 4).

Excitation source during the vibration measurement is the passing traffic and wind. Eight one-dimensional accelerometers of PCB with high sensitivity from 1054 to 1083 mV/m/s^2, were employed. The acquisition time for each setup is at least 30 minutes with a sampling frequency of 1651 Hz. Because of the limitation in number of sensors and to obtain the global vibration modes of the bridge, a measurement grid consisting of 9 setups was conducted to cover 46 measurement points on the top of deck bridge and along the bridge (see Fig. 5). However, to scale and combine these different setups, some reference points need to be chosen. The data quality at reference nodes significantly contributes to the accuracy of the system identification in the data processing step. Consequently, the locations of the reference nodes should be placed at the positions where modes of interest evidently appear. In other words, these points should not be placed at positions where modal displacements of relevant mode shapes are zero. Other roving points were spread over the bridge. Quick deployment, accessibility on-site and wire length are important factors in order to plan measurement setups. For this reason, measurement points are placed on the sidewalks; covering longitudinal, vertical, transversal directions (also see Fig. 5).

4.3 Data processing and feature extraction

A toolbox in MATLAB, namely MACEC (Reynders *et al*. 2014), is employed to process the measured data. The step-by-step signal processing procedure is performed as follows.

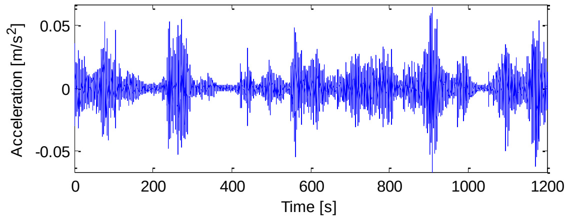

(a) Time domain

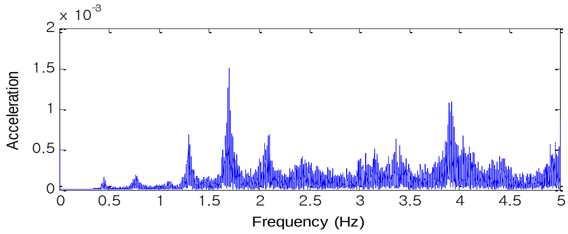

(b) Frequency domain

Fig. 6 Acceleration under ambient excitations at one sensor

4.3.1 Data pre-processing

• To remove the offsets from the measured data due to Direct Current (DC) components, "REMOVE OFFSET" function is selected with "ALL CHANNELS" options before press "APPLY".

• Low-frequency noise also needs to be removed from the data by using a "FILT-FILT" function. By entering a value of 0.1 Hz, the high-pass filter only passes signals with a frequency higher than a frequency value of 0.1 Hz.

• "TIME WINDOW" function is selected to extract only the expected pure data by defining the time window from 0 s to 1200 s, equivalent to 20 minutes of measurement.

• To save processing time, to reduce the data and to facilitate the "System Identification", "DECIMATE" function is chosen to resample the data. In general, the frequency range of interest in bridge engineering often lies between 0-20 Hz, especially the fundamental frequency values in cable-stayed bridge are quite low. By entering a decimation factor of 160, the Nyquist frequency is reduced from 800 Hz to 5 Hz.

• Using "DELETE CHANNEL" function, all data of bad signals are deleted from setup (if any).

Fig. 6(a) illustrates the time-domain response of a representative sensor. Then, Fast Fourier Transform (FFT) technique is made by transferring time-domain response to frequency-domain response as shown in Fig. 6(b). The achieved peaks in frequency domain can correspond to the natural frequencies of the bridge.

4.3.2 System identification

• Stochastic Subspace Identification (SSI) algorithm is employed to perform system identification for the output-only (also operational) Modal Analysis (OMA) of structures. By comparing two algorithms, data-driven (SSI-data) and covariance (SSI-cov), the second algorithm has some advantages: More straightforward, computationally

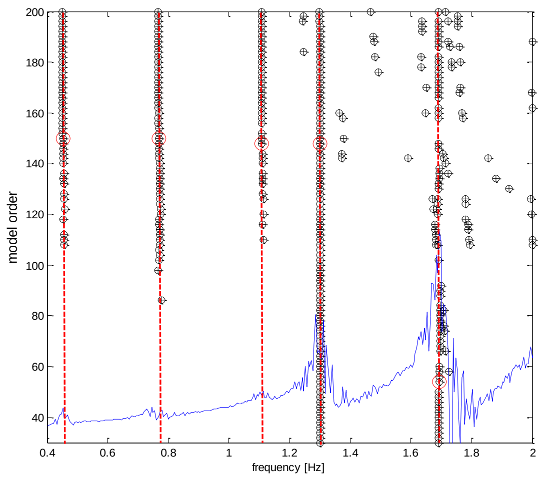

Fig. 7 Representative stabilization diagram of the bridge in an interval 0.4-2 Hz

computationally less time with a similar accuracy (Reynders *et al*. 2008). Therefore, SSI-COV is chosen to perform system identification. Details of SSI method can be found in Peeters (2000), Peeters and De Roeck (2001), Casciati *et al*. (2016) and Huang and Chen (2017).

• To kick off building of the Hankel matrix and projection matrix of measured data, an expected system order, i = 100, is entered and system matrices are calculated with system orders: 2:2:200.

4.3.3 Modal analysis

The dynamic characteristics are estimated by a stabilization diagram. Several stabilization criteria are sketched: 1% for frequency, 5% for damping factor and 1% for modal vectors. The stabilization diagrams are constructed from the state space system identified with SSI-COV as mentioned above. In Fig. 7, for a clearer view, the stabilization diagram consisting of vertical lines is shown in the interval between 0 and 2 Hz. The mode shapes of the first five modes are shown in Fig. 8.

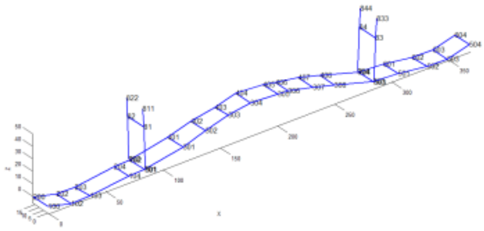

(a) Identified 1st bending mode at 0.452 Hz

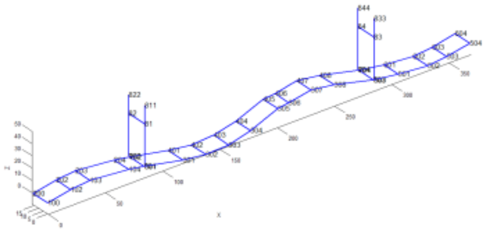

(b) Identified 2nd bending mode at 0.766 Hz

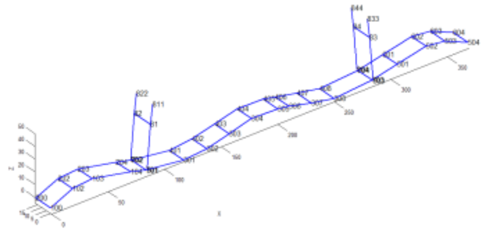

(c) Identified 3rd bending mode at 1.106 Hz

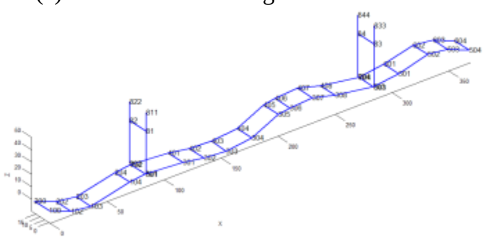

(d) Identified 4th bending mode at 1.292 Hz

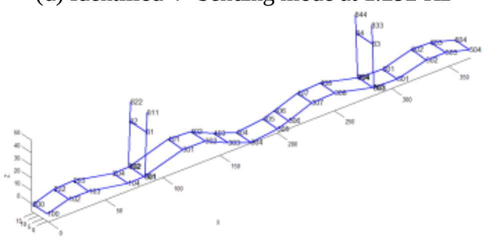

(e) Identified 5th-bending mode at 1.691 Hz

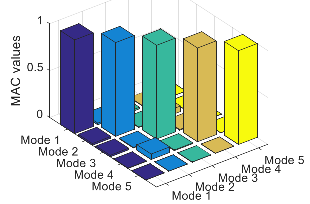

(f) MAC values

Fig. 8 Measured vertical bending modes from (a) to (e) and MAC values of the first five modes (f)

5. FE model updating

In this section, the proposed algorithms are applied for a simple pipe first and then to the Kien bridge, considering several objective functions. The obtained results are used to compare between the different methods.

5.1 Small-scale structure

The efficiency of three optimization algorithms is assessed by applying them to a pipe tested in the laboratory. Based on a report of vibration analysis of a real steel pipe conducted by Bui (2011) at KU Leuven University, the authors utilized these data to build a suitable numerical model. At first, the obtained results of numerical model are compared with measured data. Then, optimization techniques are applied to minimize the difference between simulation and measurement. Several scenarios with regard to the number of population (agents) are investigated. Convergence rate and CPU-time are used to evaluate the proposed algorithms.

5.1.1 Test descriptions

To reduce natural frequency values, two masses are

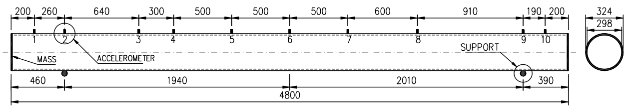

Fig. 9 Schematic drawing of experimental pipe and sensor placement (dimension in mm) (Bui 2011)

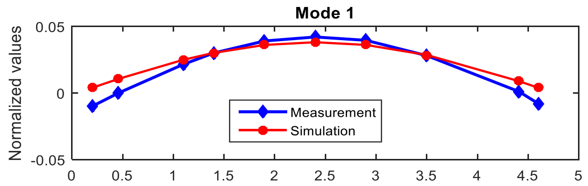

(a) The first mode

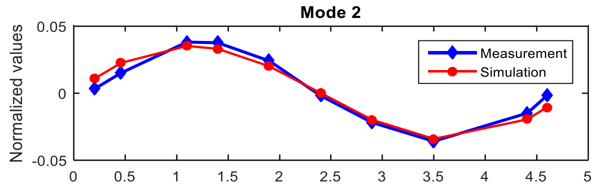

(b) The second mode

Fig. 10 Measured and simulated mode shapes of plain pipe based on 10 measurement points

Table 1 Dimensions and material properties of the pipe

Elastic modulus E (N/m^2)	Density ρ (kN/m^3)	Poisson's Ratio ν
2.1×10^{11}	7800	0.3

Table 2 Dimensions and material properties of the pipe

L (mm)	r_{out} (mm)	r_{in} (mm)	Thickness d (mm)
4800	161.925	149.225	12.7

attached at both ends of the pipe. The pipe is hanging on two flexible springs. The stiffness of the "supports" is negligible in comparison with pipe's rigidity. Thus, free-free conditions are generated. Twenty accelerometers are placed along the pipe, both on the top and side of the pipe (Fig. 9). The pipe is excited by two rotating masses placed at one pipe end. The first two vertical bending modes are identified at 34.56 Hz and 100.43 Hz. Mode shapes of plain pipe are shown in Fig. 10.

5.1.2 Numerical FE model

A FE model is built with free-free boundary condition using beam element type 189 in ANSYS (2016), which is employed to perform a dynamic analysis of the pipe. Pipe's dimensions are L = 4800 mm length, d = 12.7 mm thickness and out-diameter d_{out} = 323.85 mm (see Fig. 9). The material properties of the pipe used in the simulation are listed in Tables 1 and 2. The first two modes of simulated model are obtained and shown as Fig. 10. The first two natural frequencies and the difference in results between simulation and measurement are listed in Table 3.

From the results, it can be seen that the simulated frequencies are higher than the measured ones. It means that

Table 3 Comparison of frequency values

Mode	Natural Frequencies (Hz)		Deviation
	Experiment	Simulation	
1	34.56	35.81	-3.6%
2	100.43	105.84	-5.4%

Table 4 Variation of updating parameters in the FE model

No	Updating parameters	Initial value	Variation
1	Elastic modulus (MPa)	2.1×10^{11}	10%
2	Mass density (kg/m^3)	7800	10%

the stiffness of the FE model is overestimated. In order to decrease the error between experimental and simulated frequencies, two parameters, elastic modulus (E) and mass density (γ) are chosen for model updating. Sensitivity analysis of input parameters is not considered because of the simplicity of the model.

5.1.3 Model updating

Elastic modulus and mass density are assigned a possible change of ± 10% as listed in Table 4. Then PSO, GSA, and hybrid algorithms PSOGSA are used to identify the improved material properties. Several objective functions considering variation of frequencies, MAC, COMAC and eCOMAC values of the first two modes, are introduced to minimize the frequency deviation as follows

$$\text{Objective } 1 = \sum_{j=1}^{m}\left|1-\frac{f_{sim}^{j}\times f_{ex}^{j}}{\left(f_{ex}^{j}\right)^{2}}\right| \quad (18)$$

$$\text{Objective } 2 = \sum_{j=1}^{m}\left|1-\frac{f_{sim}^{j}\times f_{ex}^{j}}{\left(f_{ex}^{j}\right)^{2}}\right| + \sum_{j=1}^{m}\left(1-\mathrm{MAC_j}\right) \quad (19)$$

$$\text{Objective } 3 = \sum_{j=1}^{m}\left|1-\frac{f_{sim}^{j}\times f_{ex}^{j}}{\left(f_{ex}^{j}\right)^{2}}\right| + \sum_{i=1}^{n}\left(1-\mathrm{COMAC_i}\right) \quad (20)$$

$$\text{Objective } 4 = \sum_{j=1}^{m}\left|1-\frac{f_{sim}^{j}\times f_{ex}^{j}}{\left(f_{ex}^{j}\right)^{2}}\right| + \sum_{i=1}^{n}\mathrm{eCOMAC_i} \quad (21)$$

where f_{sim}, f_{ex} are simulated and experimental frequencies, respectively, m is the number of identified modes and $\mathrm{MAC_j}$ is modal assurance criterion of j^{th} mode pairs between measured and simulated data. $\mathrm{MAC_j}$ compares displacements of all nodes in each mode shape j via correlation coefficient

$$MAC_{\mathrm{j}} = \frac{\left|\sum_{i=1}^{n}(\varphi_i^{ex})^T\times\varphi_i^{sim}\right|^2}{\left\{\sum_{i=1}^{n}(\varphi_i^{ex})^T\times\varphi_i^{ex}\right\}\times\left\{\sum_{i=1}^{n}(\varphi_i^{sim})^T\times\varphi_i^{sim}\right\}} \quad (22)$$

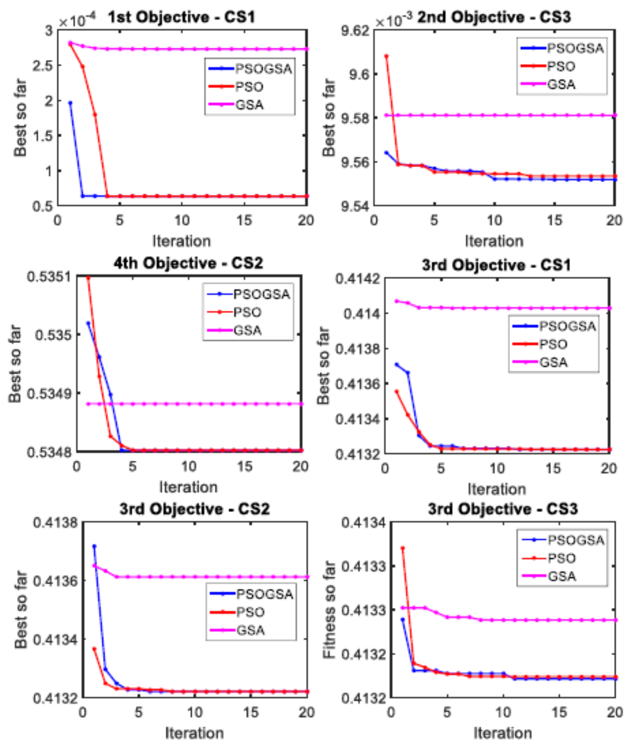

Fig. 11 Representative fitness maps of some case studies

COMAC uses at each node the displacements of all modes for comparison. It can be determined as

$$\mathrm{COMAC}_i = \frac{\left(\sum_{j=1}^{m}\left|\varphi_{j,i}^{ex} \times \varphi_{j,i}^{sim}\right|\right)^2}{\sum_{j=1}^{m}\left(\varphi_{j,i}^{ex}\right)^2 \times \sum_{j=1}^{m}\left(\varphi_{j,i}^{sim}\right)^2} \tag{23}$$

where i is node number and COMAC is co-ordinate modal assurance criterion at each node, $\varphi_{j,i}^{ex}$, $\varphi_{j,i}^{sim}$ are measured and simulated modal vectors of j^{th} mode at i^{th} node.

High values of MAC and COMAC indicate good correlation in mode pairs. Eq. (23) can be used effectively when data of mode pairs are on a similar scale. If not, a Modal Scale Factor (MSF) is suggested to scale data of mode shapes. MSF coefficient is a factor related to a pair of two-mode shapes. It is used to normalize all mode shapes of the same vibration mode to a common level. For instance, in order to scale simulated mode shapes to experimental mode shapes, $\mathrm{MSF}_{j(ex,\,sim)}$ of j^{th} mode can be calculated as

$$\mathrm{MSF}_{j(ex,\,sim)} = \frac{\sum_i^n \varphi_{i,j}^{ex} \times \left(\varphi_{i,j}^{sim}\right)^{conj}}{\sum_i^n \varphi_{i,j}^{sim} \times \left(\varphi_{i,j}^{sim}\right)^{conj}} \tag{24}$$

where n is the total number of nodes (DOFs) and *conj* implies conjugate values of mode shape data.

Therefore, the scaled value of j^{th} simulated mode shape at i^{th} node is determined by

$$\overline{\varphi}_{i,j}^{sim} = \mathrm{MSF}_{j(ex,sim)} \times \varphi_{i,j}^{sim} \tag{25}$$

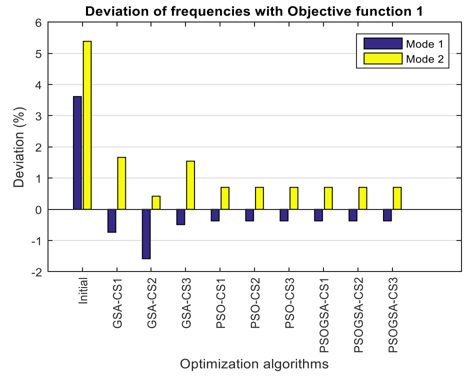

(a) Using frequencies

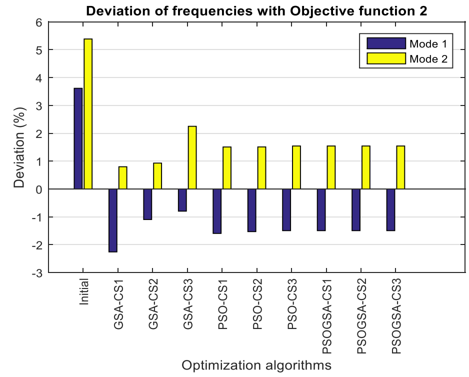

(b) Using frequencies + MAC

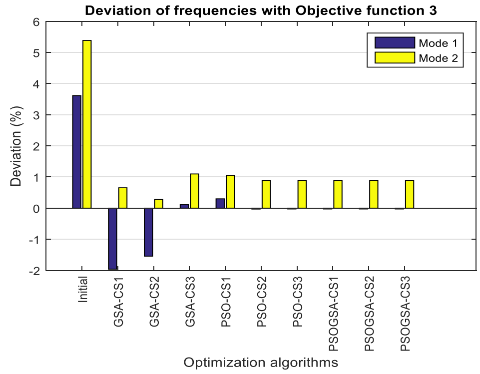

(c) Using frequencies + COMAC

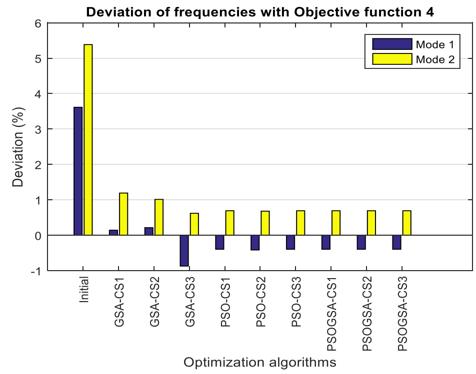

(d) Using frequencies + eCOMAC

Fig. 12 Frequency differences between simulation and measurement using three optimization algorithms

Nevertheless, COMAC parameter has inherent limitations due to scaling or polarity errors in measured data or depends on a number of identified modes that can contribute to correlation. Consequently, an enhanced

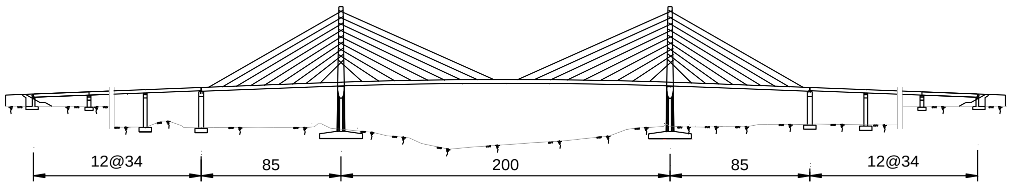

Fig. 13 General layout of Kien Bridge with fan-shaped stay cable arrangement, unit is in m

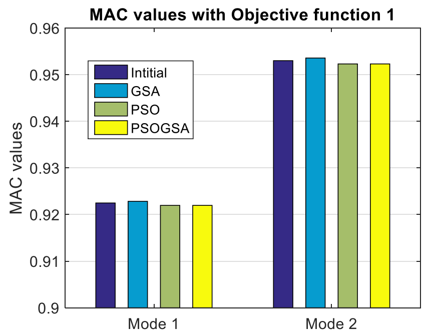

(a) Using frequencies

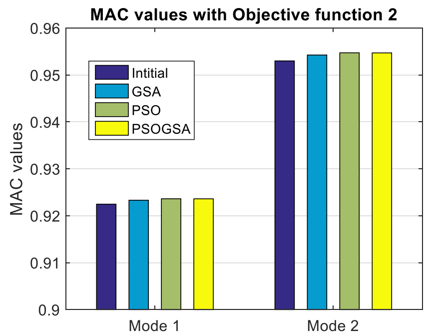

(b) Using frequecies + MAC

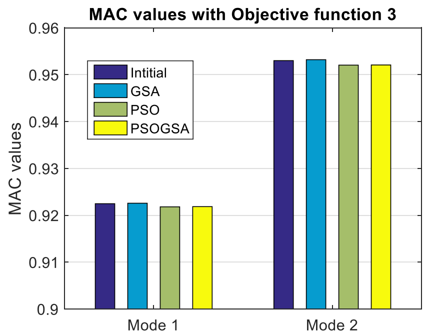

(c) Using frequecies + COMAC

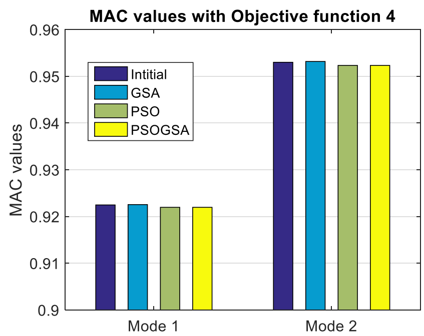

(d) Using frequecies + eCOMAC

Fig. 14 MAC values between simulation and measurement before and after updating for different objective functions

COMAC (eCOMAC) is proposed by Hunt (1992) to overcomes the drawbacks of COMAC and is calculated by using the mean of the difference of modal amplitudes of all modes for each node Chen and Ni (2018)

$$\mathrm{eCOMAC_i} = \frac{\sum_j^m \left| \varphi_{i,j}^{ex} - \overline{\varphi}_{i,j}^{sim} \right|}{2.m} \tag{26}$$

• Different pairs in the number of population (agents) and iteration (CS1: 20 and 20, CS2: 40 and 20, CS3: 80 and 20) are utilized to evaluate the feasibility of each algorithm based on updated frequencies, convergence rate, and CPU-time. Some initial parameters of these algorithms are set as follows. PSO's parameters are w = 0.9, c_c = c_s = 2. GSA's factors are α = 20, G_0 = 100. PSOGSA's parameters are set to c_c = 0.5, c_s = 1.5, α = 20, G_0 = 1. The maximum discrepancies in frequencies after updating significantly reduce under 2.2% for GSA, 1.5% for PSO and PSOGSA, especially when using only frequency or a combination of frequency and eCOMAC/COMAC as shown in Fig. 12.

The convergence of these algorithms is shown in Fig. 11 related to the changes in number of agents (particles) as well as objective functions as mentioned above. From the obtained fitness maps, PSO and PSOGSA show their potential and effectiveness in estimating the updating parameters thanks to their good convergence. Both algorithms show similar computational costs associated with variance of population (number of particles/agents) (Fig. 13). Although GSA reveals a slight inferior performance, it also improves its convergence at a higher population.

It is obvious that the updated frequencies are much closer to the measured frequencies than the initial values. Besides that, from the graphs, PSO and PSOGSA show stable and superior performance in comparison with GSA, when they are applied to predict the updating parameters. *MAC* values between mode pairs are increased slightly when a combination of frequency and MAC is considered, while other functions obtain lower values of MAC (see Fig. 14).

From the obtained results, PSO and PSOGSA are good algorithms for updating uncertain values of material in the FE model by minimizing the difference between experimental and numerical data. The higher exploitation of PSOGSA and PSO compared to GSA is because PSOGSA, PSO have social components. This allows PSOGSA, PSO to exploit around the best obtained mass so far. In GSA, the heavy masses have better values of fitness function. After finding a promising solution, these masses gather around the solution for exploitation. In the final steps of iterations, when masses gather around the promising solution, they

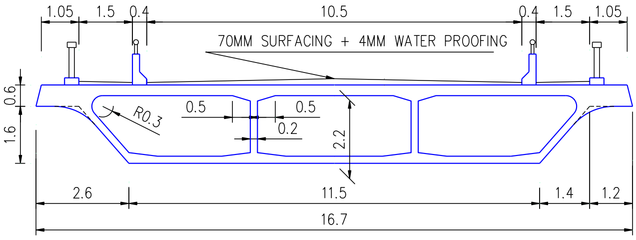

(a) Typical cross-section of bridge

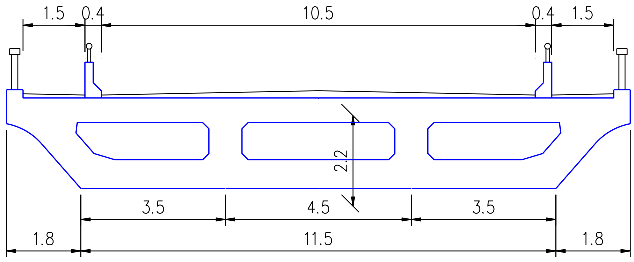

(b) Cross-section of bridge at pylon

Fig. 15 Cross section of main girders. Unit is in m

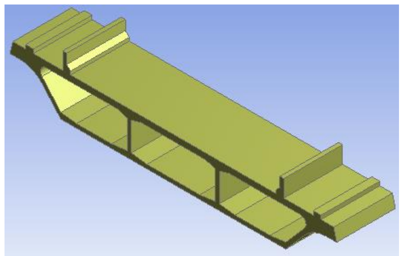

Fig. 16 A typical segment model in ANSYS

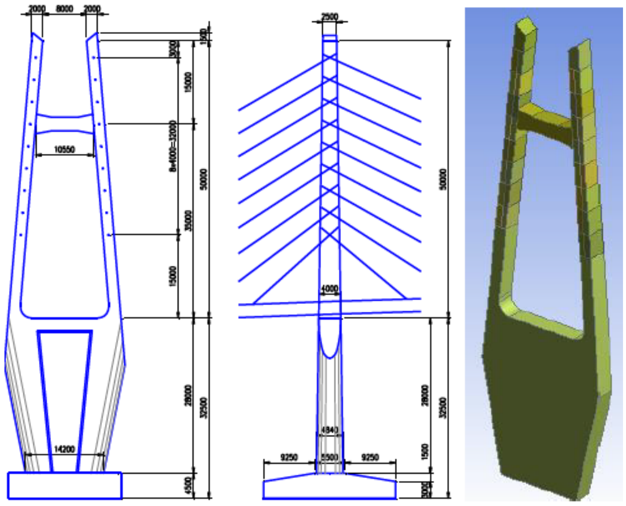

Fig. 17 General layout of the pylon and pylon model. Unit is in mm

have almost the same weights. Due to this reason, gravitational forces of approximately same intensity attract each other. For this reason, GSA does not achieve good results as the other algorithms. Besides, it seems that GSA can be trapped in local minima instead of searching a global minimum. This can be seen in Fig. 11. The fitness values obtained by GSA change negligibly and almost vary in the vicinity of the first value.

From the obtained results above, PSO and PSOGSA are good algorithms for updating uncertain values of material in the FE model by minimizing the difference between experimental and numerical data. However, their potential still has to be investigated in a real structure. Besides that, multiple-objective function of frequency and MAC (OF2) shows its efficiency when used to update the FE model. Results of both frequency and MAC values are improved while other choices of objective function achieved only an improvement in frequencies (see Figs. 12 and 14).

5.2 Large-scale Kien cable-stayed bridge

5.2.1 Initial model

The main cable stayed Kien bridge having three spans (85 m + 200 m + 85 m) is modelled using ANSYS (2016). The obtained results of the initial FE model are used as a reference to plan the measurement setups. Only the main box-girder bridge is used to build a FE model for comparison with measured data.

• Main girder: The main box girder is modelled using 3D 8-node solid elements. Eight nodes are used to define the element. Each node has three degrees of freedom (DOFs): translations in the nodal X, Y and Z directions.

Fig. 15. non-structural elements like handrail, asphalt pavement are defined on the element faces as added mass. The concrete parapets and barriers are modelled with solid elements as part of the box girder (see Fig. 16).

• Pylon: Pylon is also modelled with 3D-8 node solid elements as the main girder. The upper pylon cross-section has a slight change in the vertical direction and is divided into 9 elements at the cable anchoring points. The division of the upper pylon is to facilitate modelling of the cables.

The pylon section changes from 5.5 m at the bottom to 2.5 m at the top. To simplify, an averaged value at 4 m is used to model the axial dimension of pylon. For further study, the pylon will be modelled with the real dimension in as-built drawings (see Fig. 17).

• Cables: Boundary conditions: Kien bridge consists of 72 cables on both sides. Cables of the bridge are modelled by link 180 elements. The element is a uni-axial tension-compression element with three degrees of freedom at each node: translations in the nodal X, Y and Z directions. Each cable is modelled by one element and is rigidly connected with pylon and main girder. Tension-only function is chosen for modelling cables. The parameters of the cable are listed in Table 5.

The pylon leg is completely fixed (Fig. 18). Steel-laminated rubber bearings are supporting the bridge at the end-span and at the pylon. They are modelled with 3D-8 nodes solid elements using orthotropic properties as presented in Table 5.

• Results of FE model: Based on as-built drawings, initial values of material properties and boundary conditions, free vibration of the bridge is analyzed by ANSYS®. The first eight modes are extracted, including six vertical bending modes, one horizontal bending mode, and one torsion mode. Mode shapes and the corresponding

Table 5 List of 20 parameters and their variation ranges ± Δ%

Parameter	Symbol	Initial value
Main girder - Δ = 5%		
1. Young modulus of concrete	E-beam	36,057
2. Density of concrete, Δ = 10%	Density-beam	2,700
3. Poisson's ratio of concrete	Pr-beam	0.2
Pylon - Δ = 5%		
4. Young modulus of concrete	E-pylon	31,975
5. Density of concrete	Density-pylon	2,500
6. Poisson's ratio of concrete	Pr-pylon	0.2
Cable stay - Δ = 5%		
7. Young modulus of cable	E-cable	197,000
8. Density of cable	Density-cable	7,850
9. Poisson's ratio of cable	Pr-cable	0.3
10. Sectional area of stay type 1	r1-cable	0.00672
11. Sectional area of stay type 2	r2-cable	0.00518
Bearings - Δ = 5%		
12. Young modulus - *x* direction	E-bearing-*x*	189,000
13. Young modulus - *y* direction	E-bearing-*y*	1,890
14. Young modulus - *z* direction	E-bearing-z	1,890
15. Shear modulus - *x* direction	G-bearing-*x*	71,370
16. Shear modulus - *y* direction	G-bearing-*y*	64,233
17. Shear modulus - *z* direction	G-bearing-*z*	60,665
18. Poisson's ratio - *x* direction	Pr-bearing-*x*	0.25
19. Poisson's ratio - *y* direction	Pr-bearing-*y*	0.3
20. Poisson's ratio - *z* direction	Pr-bearing-*z*	0.35

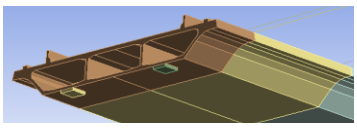
(a) At the end-span
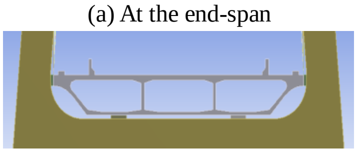
(b) At the pylon
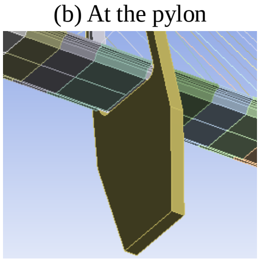
(c) Pylon leg

Fig. 18 Boundary conditions

frequencies are shown in Fig. 19. Discrepancies of frequencies between experiment and simulation are listed in Table 6 with the maximum deviation up to 13.09%.


(a) Mode 1 (0.477 Hz)
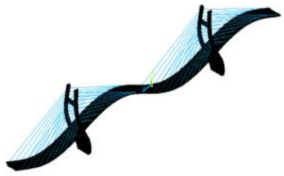
(b) Mode 2 (0.806 Hz)
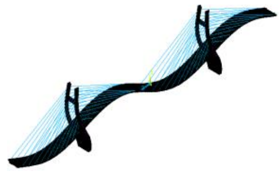
(c) Mode 3 (1.022 Hz)
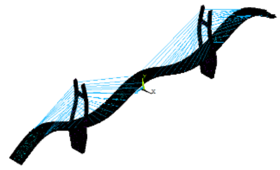
(d) Mode 4 (1.252 Hz)
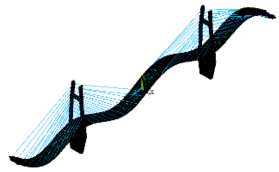
(e) Mode 5 (1.373 Hz)
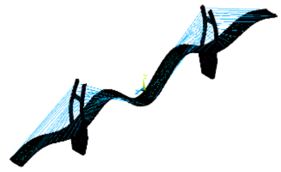
(f) Mode 6 (1.589 Hz)
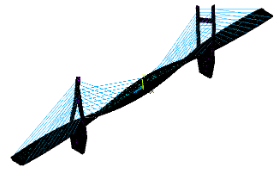
(g) Mode 7 (1.887 Hz)
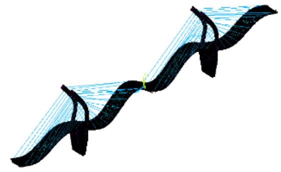
(h) Mode 8 (2.522 Hz)

Fig. 19 Simulated mode shapes extracted from the FE model - Kien cable-stayed bridge

Table 6 The first five bending natural frequencies

Mode	Measured	Initial – FE model	Deviation
1	0.452	0.477	5.60%
2	0.766	0.806	5.22%
3	1.107	1.252	13.09%
4	1.293	1.373	6.22%
5	1.691	1.589	-6.06%

5.2.2 Calibrated model

The deviation in frequencies between measured and extracted from the initial FE model varies from -6.06% to 13.09%. To achieve a better result, the FE model needs to be calibrated. The effects of approach piers, as well as successive spans to the dynamic behaviour of the cable-stayed bridge are considered. In order to achieve results that are closer to the behaviour of bridge, the initial FE model is modified by modelling asphalt layers on top of deck with real depth. The approach piers and spans are added in the new model. Moreover, local components like hollow diaphragms between two girder segments are also simulated as shown in Figs. 20-22. These changes can contribute to total stiffness of the bridge.

Based on the changes above, new frequencies are calculated by ANSYS as shown in Table 7. It is observed that the obtained frequencies of the calibrated FE model are closer to the experimental ones than those of the initial FE model. The highest discrepancy is only 9.2% in the third

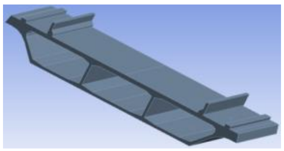

(a) Using equivalent load in initial FE model

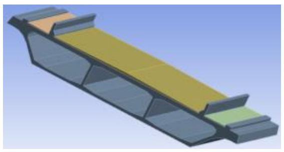

(b) Modelling real depth of asphalt layers

Fig. 20 Effects of asphalt layers

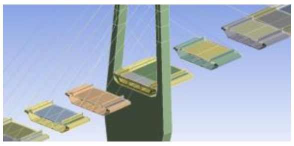

(a) Ignoring diaphragms

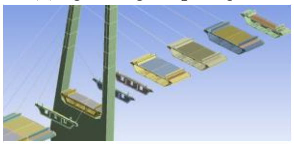

(b) Modelling hollow diaphragms

Fig. 21 Effects of hollow diaphragms

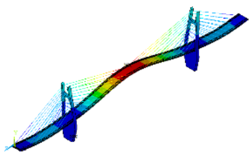

(a) Without approach piers

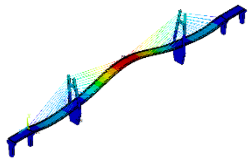

(b) Simulating approach piers and spans

Fig. 22 Effects of approach piers and spans

Table 7 Comparison between experimental and calibrated FE model

Mode	Measured	Calibrated FE model	Deviation
1	0.452	0.464	2.57%
2	0.766	0.765	-0.19%
3	1.107	1.209	9.20%
4	1.293	1.345	4.00%
5	1.691	1.574	-6.90%

mode.

As there are many parameters in FE model that can influence the accuracy of outputs, a proper selection of updating parameters is indispensable. For this reason, a sensitivity analysis is carried out hereinafter to identify the most effective parameters that can be used in the updating procedure. As mention above, due to dominant computational burden, Morris method is used to determine the most important updating parameters.

5.2.3 Sensitivity analysis (SA)

In a large, long-span structure as a cable-stayed bridge, the identified frequencies under the ambient excitation, e.g. vehicle, wind, earthquake, etc., reach often low values (Reynders and Roeck 2008). These low modes often represent the global behaviour of the structure. The first few modes are most often used for model updating.

For a real, complex structure, many uncertain parameters can affect the outputs of a FE model, e.g., frequencies and mode shapes. The modified mean sensitivity index, μ*, from Morris screening method examines the contribution of each input parameter to the outputs of interest in the FE model. The higher value of the index, the more significant impact of the parameter is. These values are then used to exclude parameters with negligible effect from the set of updating parameters based on explicit calculation instead of engineering's experience. A reasonable number of updating parameters compared to the number of error values in the fitness function can guarantee the accuracy and the uniqueness of the solution of model updating process.

For sensitivity analysis, the effect of each input parameter on each separate part of the objective functions was investigated. The obtained results reveal the number of the key input parameters and how much impact they have on each error in the objective function. Therefore, on one hand, local effects of these parameters to each frequency are investigated. On the other hand, to generate a fundamental base for updating procedure, influences of them are considered with regard to four objective functions as follows

$$\mathrm{OF1} = \sum_{j=1}^{m} \left| 1 - \frac{f_{sim}^{j} \times f_{ex}^{j}}{\left(f_{ex}^{j}\right)^{2}} \right| \tag{27}$$

$$\mathrm{OF2} = \sum_{j=1}^{m} (1 - \mathrm{MAC_j}) \tag{28}$$

$$\mathrm{OF3} = \sum_{i=1}^{n} (1 - \mathrm{COMAC_i}) \tag{29}$$

$$\mathrm{OF4} = \sum_{i=1}^{n} \mathrm{eCOMAC_i} \tag{30}$$

A random set of input parameters from the considered variation is generated in the first step. Then, forming a *m-by-k* sampling matrix with k = 20 input variables, $m = k + 1$ = 21 runs (simulations) are required. According to Morris' experiments, number of variables (or number of level) p = 4, number of trajectory r = 4 and variation size (or sampling step) $\Delta = p/[2(p - 1)] = 2/3$ are chosen.

From the changes in input parameters, outputs of the

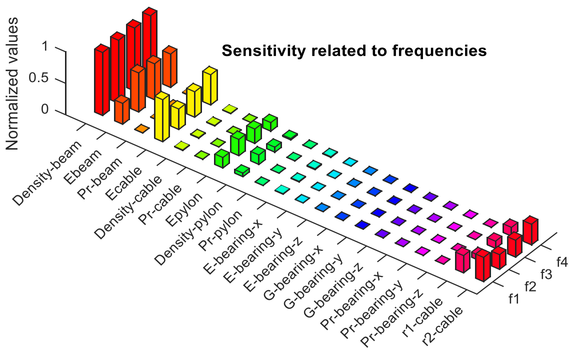

(a) Using frequencies

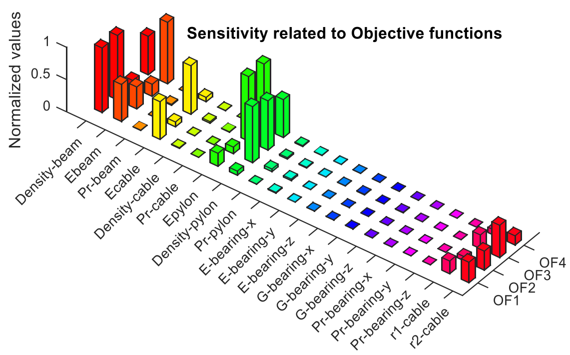

(b) Using objective functions

Fig. 23 Normalized sensitivity of 20 updating parameters

Table 8 List of updating factors after sensitivity analysis

Updating parameters	Initial value	Upper allowance	Lower allowance
E-beam	36,057	37,859	34,254
Density-beam	2,700	2,970	2,430
E-pylon	31,975	33,574	30,377
Density-pylon	2,500	2,625	2,375
E-cable	197,000	206,850	187,150
r1-cable	0.00672	0.007056	0.006384
r2-cable	0.00518	0.005439	0.004921

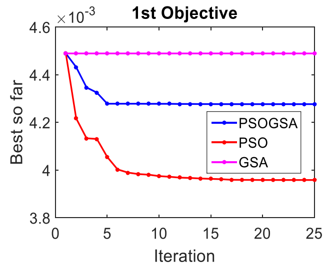

(a) Using frequencies (OF1)

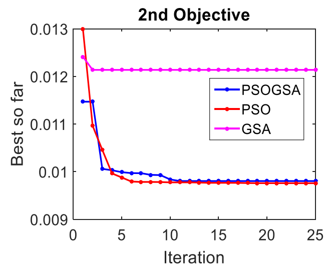

(b) Using frequencies + MAC (OF2)

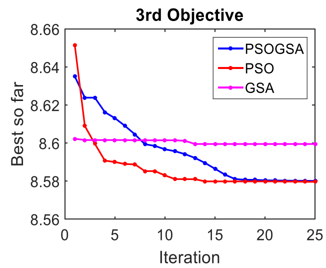

(c) Using frequencies + COMAC (OF3)

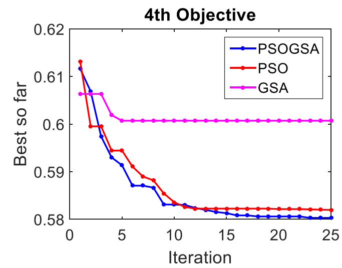

(d) Using frequencies + *eCOMAC* (OF4)

Fig. 24 Fitness with respect to different objective functions and optimization algorithms

simulation are calculated associated with separate objectives. The obtained values of modified mean sensitivity index μ^* of each factor are revealed in Fig. 23. In order to facilitate the readers having a simple and visual view of the important role of each input parameter, the normalized values of sensitivity indices are shown.

From the sensitivity magnitudes of factors related to corresponding objectives, it is obvious that seven parameters can be chosen as updating parameters: the three Young moduli of concrete main girder, pylon and steel cable, the two concrete densities of main girder and pylon, and the diameters of 2 stays. The 20 factors are shortened to 7 parameters as shown in Table 8. The step-by-step updating procedure is described in the next section.

5.2.4 Model updating

From the results of sensitivity analysis, seven parameters are chosen for model updating based on the first four modes. These parameters are considered by applying PSO, GSA and hybrid algorithm PSOGSA in combination with different objective functions. For the large-scale bridge, four fitness functions are calculated. The first objective function is only based on the frequencies, while the three others use a combination between frequencies and MAC or COMAC or eCOMAC values. These objective functions (case studies – CS) are shown in Eqs. (18) to (21). The normalized values of mode shapes fall in a range [0-1], using the Modal Scale Factors (MSF) as presented in Eq. (24).

The cable-stayed bridge in the study is a typical representative of a computationally demanding analysis because almost all components of the bridge are modelled by 3D-solid elements. Therefore, a maximum number of iterations of 25 and a number of particles of 25 are set in the optimization procedure.

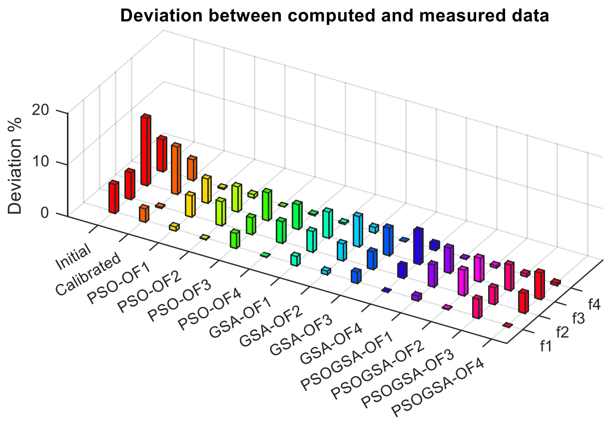

Fig. 25 Comparison of frequencies between the first four updated modes with regard to optimization algorithms and objective functions

Table 9 Summarization of error of frequency between measurement and simulation (%)

Mode	PSO			
	OF1	OF2	OF3	OF4
1	-0.77	0.14	2.99	-0.09
2	-4.11	4.90	3.35	-4.19
3	4.70	-4.63	-5.14	4.82
4	-0.22	-0.66	-0.02	0.19
Mode	GSA			
1	-1.82	0.69	2.22	-0.02
2	-3.99	3.40	3.53	-2.46
3	5.06	-5.57	-5.06	6.44
4	-0.27	-1.05	-0.03	1.33
Mode	PSOGSA			
1	-0.96	0.14	3.86	-0.02
2	-4.27	5.22	3.35	-3.89
3	4.86	-4.39	-4.75	5.12
4	-0.12	-0.46	0.58	0.48

Table 10 MAC values obtained using PSOGSA associated with the 4 objective functions

Mode	Initial	OF1	OF2	OF3	OF4
1	0.995	0.996	0.996	0.996	0.996
2	0.982	0.988	0.991	0.987	0.990
3	0.965	0.987	0.985	0.989	0.988
4	0.925	0.905	0.935	0.911	0.929

The input parameters of optimization algorithms are the same as those used in the plain pipe example. The computational costs of twelve simulation runs of three algorithms and four objective functions are plotted in Fig. 24.

• The convergence rate of individual algorithms is different with respect to each objective function. PSO and PSOGSA, especially PSO, continue to perform better than GSA, with faster convergence and a smaller value of fitness. Explanation of these results is similar to that mentioned above in the results of the small-scale structure example. From Fig. 24, the first and the second objective functions have a quick convergence in comparison with the two others. This is because the first function only uses data of frequencies and the second function uses data of frequency and five values of MAC. Besides using data of frequencies, functions 3 or 4 have to employ data of COMAC or eCOMAC at 16 points along the bridge. Therefore, it is understandable why they take more time for convergence.

Table 11 MAC values obtained using PSO associated with the 4 objective functions

Mode	Initial	OF1	OF2	OF3	OF4
1	0.995	0.996	0.996	0.996	0.996
2	0.982	0.989	0.991	0.986	0.990
3	0.965	0.984	0.985	0.985	0.987
4	0.925	0.916	0.935	0.896	0.927

Table 12 MAC values obtained using GSA associated with the 4 objective functions

Mode	Initial	OF1	OF2	OF3	OF4
1	0.995	0.996	0.996	0.996	0.996
2	0.982	0.988	0.989	0.988	0.989
3	0.965	0.928	0.988	0.989	0.989
4	0.925	0.901	0.922	0.908	0.920

• Fig. 25 illustrates the error of frequencies between simulation and experiment with respect to different objective functions. Details of the error in percentage are listed in Table 9.

• After updating, the distance between computed and experimental frequencies is decreased from maximum error at 9.2% (Table 7) to under 6.44% in the third mode. The errors in frequencies of the first and the fourth mode are reduced significantly. The second mode is not well predicted. Frequencies with respect to PSO and PSOGSA (maximum error of |5.14%|, |5.12%|, respectively) are closer to the measured frequency than GSA (maximum error of |6.44%|).

• From the Table 9, almost the smallest deviation of frequencies can be achieved by using COMAC, and eCOMAC in the objective function. Tables 10, 11, 12 indicate that the use of MAC, and eCOMAC in the objective function can achieve better value of MAC. In other words, the correlation between the mode shapes of simulation and experiment was improved when using MAC, and eCOMAC. In general, among these indices, eCOMAC has a superior performance related to improving both frequencies and mode shapes. Using only frequencies in objective function is not able to achieve good results for both frequencies and mode shapes.

• In comparison with the mode shapes from the initial model, the updated mode shapes of the first three modes are

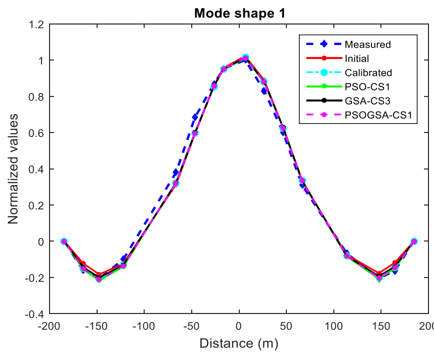

(a) The 1st vertical bending mode

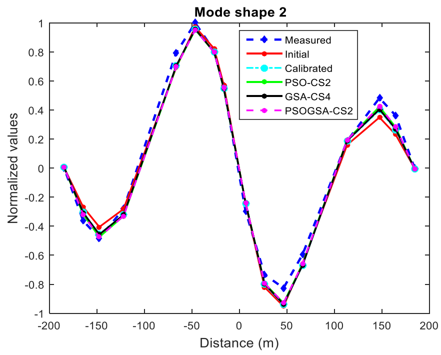

(b) The 2nd vertical bending mode

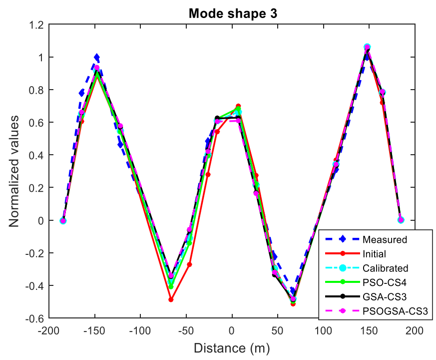

(c) The 3rd vertical bending mode

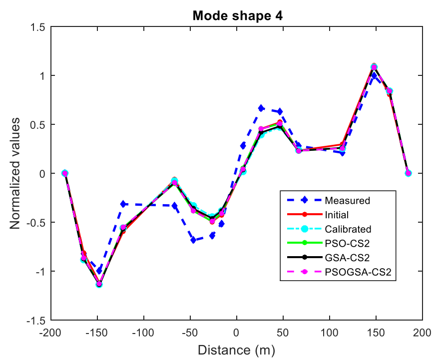

(d) The 4th vertical bending mode

Fig. 26 Comparison between simulated mode shapes and measured mode shapes for the first four vertical bending modes

improved significantly. Although the obtained shape of the fourth mode is ameliorated, the level of enhancement is negligible. Fig. 26 is used to perform the visual correlation of pairs of mode shapes between measurement and simulation. For correlation quantification, MAC is used to determine the similarity of two mode shapes. A value of one shows a perfect match. In this study, MAC values for the first four vertical bending modes after updating are shown in Tables 10-12. It can be seen that the first three modes provide a superior match between calculated and simulated mode shapes. MAC values of these modes are over 0.985. The fourth mode shows a worse value than other modes, however, this value is still acceptable in practical applications. In this measurement, because of the limitation of accelerometers, 9 setups, each setup consists of eight sensors, were used to cover all measurement points along the bridge. Besides ambient effects, the time delay and synchronization between two setups can cause this mismatch. Moreover, in this four-day measurement campaign, sensors were removed after each day. Reinstallation of sensors on the bridge in the next day, especially at reference points (indispensable points to combine two successive setups), can contribute to the error. To improve the results, measurement grid should be increased by using a larger number of accelerometers, and thus reducing the number of setups.

• Objective function based on frequency and MAC or eCOMAC index shows better results in term of frequencies and mode shapes than the others although these approaches need more time for simulation runs than the others need (see Table 13).

Table 13 Comparison of required time for each run for different objective functions and algorithms

Algorithms	Runtime in hour			
	OF1	OF2	OF3	OF4
PSO	30.44	30.69	30.25	30.94
GSA	30.18	30.55	30.33	31.84
PSOGSA	30.49	30.94	30.25	31.01

6. Conclusions

This paper investigated the effectiveness and reliability of three metaheuristic optimization techniques using several objective functions for a small-scale laboratory pipe and the Kien cable-stayed bridge.

• The application of sensitivity analysis into the model updating of the Kien bridge reveals a comprehensive view of the influence of updating parameters on the FE results. It contributes to a significant reduction of CPU-time by eliminating 13 less important parameters from 20 surveyed parameters, so finally retaining 7 updating parameters for model updating.

• PSO demonstrates efficiency and reliability due to its convergence rate and accuracy when applied to real complex structures like the Kien bridge, representing computationally demanding FE model updating problem.

• The fitness between the simulation and the measurement is improved by applying objective functions which include MAC, COMAC and eCOMAC. The errors of the frequencies and the mode shapes between simulation and measurement are minimized.

• The good results of objective functions show the great potential of applying COMAC and eCOMAC indicators in the assessment of structural damage by a modal-based approach.

The obtained results could be utilized to build the baseline FE model for the Kien cable-stayed bridge. Based on this model, some activities will be conducted in the future for structural health monitoring e.g., predicting dynamic behaviour, detecting and locating potential defects, and making a decision on maintenance based on vibration responses.

Acknowledgments

The authors acknowledge the financial support of VLIR-OUS TEAM Project, VN2018TEA479A103, 'Damage assessment tools for Structural Health Monitoring of Vietnamese infrastructures', funded by the Flemish Government.

Authors would like to express appreciation to colleagues from UCT company for supporting the measurement. Dr. Phuc Phung Van, Dr. Tien Dung Dinh and Mr. Duy Khuong Nguyen from Ghent University for their consultancies.

References

Altunisik, A.C. and Bayraktar, A. (2017), "Manual model updating of highway bridges under operational condition", *Smart Struct. Syst., Int. J.*, **19**(1), 39-46. https://doi.org/10.12989/sss.2017.19.1.039.

Anitescu, C., Atroshchenko, E., Alajlan, N. and Rabczuk, T. (2019), "Artificial neural network methods for the solution of second order boundary value problems", *Comput. Mater. Contin.*, **59**(1), 345-359. https://doi.org/10.32604/cmc.2019.06641.

Boscato, G., Salvatore, R., Ceravolo, R. and Fragonara, L.Z. (2015), "Global sensitivity-based model updating for heritage structures: Global sensitivity-based model updating for heritage structures", *Comput. Aided Civ. Infrastruct. Eng.*, **30**(8), 620-635. https://doi.org/10.1111/mice.12138.

Bui, T.T. (2011), "Experimental report of a plain pipe", Report No 01, Department of Civil Engineering, KU Leuven, Belgium.

Campolongo, F., Cariboni, J. and Saltelli, A. (2007), "An effective screening design for sensitivity analysis of large models", *Environ. Model. Softw.*, **22**(10), 1509-1518. https://doi.org/10.1016/j.envsoft.2006.10.004.

Carvalho, J., Datta, B.N., Gupta, A. and Lagadapati, M. (2007), "A direct method for model updating with incomplete measured data and without spurious modes", *Mech. Syst. Signal Process.*, **21**(7), 2715-2731. https://doi.org/10.1016/j.ymssp.2007.03.001.

Casciati, F., Casciati, S., Elia, L. and Faravelli, L. (2016), "Optimal reduction from an initial sensor deployment along the deck of a cable-stayed bridge", *Smart Struct. Syst., Int. J.*, **17**(3), 523-539. https://doi.org/10.12989/sss.2016.17.3.523.

Chen, H.P and Ni, Y.Q. (2018), *Structural Health Monitoring of Large Civil Engineering Structures*, John Wiley & Sons Ltd, Chichester, West Sussex, UK.

Cottin, N. and Reetz, J. (2006), "Accuracy of multiparameter eigenvalues used for dynamic model updating with measured natural frequencies only", *Mech. Syst. Signal Process.*, **20**(1), 65-77. https://doi.org/10.1016/j.ymssp.2004.10.005.

Deng, Lu. and Cai, C.S. (2010), "Bridge model updating using response surface method and genetic algorithm", *J. Bridge Eng.*, **15**(5), 553-564. https://doi.org/10.1061/(ASCE)BE.1943-5592.0000092.

Feng, K., Lu, Z. and Yang, C. (2019), "Enhanced Morris method for global sensitivity analysis: Good proxy of Sobol' index", *Struct. Multidiscipl. Optim.*, **59**(2), 373-387. https://doi.org/10.1007/s00158-018-2071-7.

Huang, T.L. and Chen, H.P. (2017), "Mode identifiability of a cable-stayed bridge using modal contribution index", *Smart Struct. Syst., Int. J.*, **20**(2), 115-126. https://doi.org/10.12989/sss.2017.20.2.115.

Hamdia, K.M., Ghasemi, H., Zhuang, X., Alajlan, N. and Rabczuk, T. (2018), "Sensitivity and uncertainty analysis for flexoelectric nanostructures", *Comput. Methods Appl. Mech. Eng.*, **337**, 95-109. https://doi.org/10.1016/j.cma.2018.03.016.

Hamdia, K.M., Silani, M., Zhuang, X., He, P. and Rabczuk, T. (2017), "Stochastic analysis of the fracture toughness of polymeric nanoparticle composites using polynomial chaos expansions", *Int. J. Fract.*, **206**, 215-227. https://doi.org/10.1007/s10704-017-0210-6.

Hoa, T.N., Khatir, S., De Roeck, G., Long, N.N., Thanh, B.T. and Wahab, M.A. (2020), "An efficient approach for model updating of a large-scale cable-stayed bridge using ambient vibration measurements combined with a hybrid metaheuristic search algorithm", *Smart Struct. Syst., Int. J.*, **25**(4), 487-499. https://doi.org/10.12989/sss.2020.25.4.487

Hunt, D.L. (1992), "Application of an enhanced coordinate modal assurance criterion", *Proceedings of the 10th International Modal Analysis Conference*, San Diego, CA, USA, February.

Islam, M.S., Do, J. and Kim, D. (2018), "Vibration control of offshore wind turbine using RSM and PSO-optimized Stockbridge damper under the earthquakes", *Smart Struct. Syst., Int. J.*, **21**(2), 207-223. https://doi.org/10.12989/sss.2018.21.2.207.

Ghiasi, R. and Ghasemi, M.R. (2018), "Optimization-based method for structural damage detection with consideration of uncertainties- a comparative study", *Smart Struct. Syst., Int. J*, **22**(5), 561-574. https://doi.org/10.12989/sss.2018.22.5.561.

Kennedy, J. and Eberhart, R. (1995), "Particle swarm optimization", *Proceedings of ICNN'95 - International Conference on Neural Networks*, Perth, WA, Australia, December.

Khatir, S., Wahab, M.A., Boutchicha, D., Capozucca, R. and Khatir, T. (2019), "Optimization of IGA parameters based on beam structure using cuckoo search algorithm", *Proceedings of the 1st International Conference on Numerical Modelling in Engineering*, Singapore, August.

Khatir, S., Wahab, M.A., Boutchicha, D. and Khatir, T. (2019), "Structural health monitoring using modal strain energy damage indicator coupled with teaching-learning-based optimization algorithm and isogoemetric analysis", *J. Sound Vib.*, **448**, 230-246. https://doi.org/10.1016/j.jsv.2019.02.017.

Khatir, S., Dekemele, K., Loccufier, M., Khatir, T. and Wahab, M.A. (2018), "Crack identification method in beam-like structures using changes in experimentally measured frequencies and particle swarm optimization", *Comptes Rendus Mécanique*, **346**(2), 110-120. https://doi.org/10.1016/j.crme.2017.11.008.

Khatir, S., Khatir, T., Boutchicha, D., Le Thanh, C., Tran-Ngoc, H., Bui, T.Q., Capozucca, R. and Abdel-Wahab, M. (2020), "An efficient hybrid TLBO-PSO-ANN for fast damage identification in steel beam structures using IGA", *Smart Struct. Syst., Int. J.*, **25**, 605-617. https://doi.org/10.12989/sss.2020.25.5.605.

Le-Duc, T., Nguyen, Q.H. and Nguyen-Xuan, H. (2020), "Balancing composite motion optimization", *Inf. Sci.*, **520**, 250-270. https://doi.org/10.1016/j.ins.2020.02.013.

Lin, R.M. and Ewins, D.J. (1994), “Analytical model improvement using frequency response functions”, *Mech. Syst. Signal Process.*, **8**(4), 437-458. https://doi.org/10.1006/mssp.1994.1032.

Menberg, K., Heo, Y. and Choudhary, R. (2016), “Sensitivity analysis methods for building energy models: Comparing computational costs and extractable information”, *Energy Build.*, **133**, 433-445. https://doi.org/10.1016/j.enbuild.2016.10.005.

Mirjalili, S., Wang, G.G. and Coelho, L.S. (2014), “Binary optimization using hybrid particle swarm optimization and gravitational search algorithm”, *Neural Comput. Appl.*, **25**(6), 1423-1435. https://doi.org/10.1007/s00521-014-1629-6.

Morris, M.D. (1991), “Factorial sampling plans for preliminary computational experiments”, *Technimetrics*, **33**(2), 161-174. https://doi.org/10.2307/1269043.

Peeters, B. (2000), “System identification and damage detection in civil engineering”, Ph.D. Dissertation, Katholieke Universiteit Leuven, Belgium.

Peeters, B. and De Roeck, G. (2001), “Stochastic system identification for operational modal analysis: A review”, *J. Dyn. Syst. Meas. Control*, **123**(4) 659-667. https://doi.org/10.1115/1.1410370.

Qin, S., Zhang, Y., Zhou, Y.L. and Kang, J. (2018), “Dynamic model updating for bridge structures using the kriging model and PSO algorithm ensemble with higher vibration modes”, *Sensors*, **18**(6), 1879. https://doi.org/10.3390/s18061879.

Rashedi, E., Nezamabadi-pour, H. and Saryazdi, S. (2009), “GSA: A gravitational search algorithm”, *Inf. Sci.*, **179**(13), 2232-2248. https://doi.org/10.1016/j.ins.2009.03.004.

Reynders, E., Schevenels, M. and De Roeck, G. (2014), “A MATLAB toolbox for experimental and operational modal analysis”, MACEC 3.2, Department of Civil Engineering, KU Leuven, Belgium.

Reynders, E., Pintelon, R. and De Roeck, G. (2008), “Uncertainty bounds on modal parameters obtained from stochastic subspace identification”, *Mech. Syst. Signal Process.*, **22**(4) 948-969. https://doi.org/10.1016/j.ymssp.2007.10.009.

Reynders, Ed. and De Roeck, G. (2008), “Reference-based combined deterministic–stochastic subspace identification for experimental and operational modal analysis”, *Mech. Syst. Signal Process.*, **22**(3) 617-637. https://doi.org/10.1016/j.ymssp.2007.09.004.

Saltelli, A. (2004), *Sensitivity Analysis in Practice: A Guide to Assessing Scientific Models*”, John Wiley & Sons Ltd, Chichester, West Sussex, UK.

Sobol, I.M. (2001), “Global sensitivity indices for nonlinear mathematical models and their Monte Carlo estimates”, *Math. Comput. Simul.*, **55**(1-3) 271-280. https://doi.org/10.1016/S0378-4754(00)00270-6.

ANSYS (2016), ANSYS Mechanical Release 17.0, ANSYS Inc.

Tran-Ngoc, H., He, L., Reynders, E., Khatir, S., Le-Xuan, T., De Roeck, G., Bui-Tien, T. and Abdel Wahab, M. (2020), “An efficient approach to model updating for a multispan railway bridge using orthogonal diagonalization combined with improved particle swarm optimization”, *J. Sound Vib.*, **476**, 115315. https://doi.org/10.1016/j.jsv.2020.115315.

Tran-Ngoc, H., Khatir, S., De Roeck, G., Bui-Tien, T., Nguyen-Ngoc, L. and Abdel Wahab, M. (2018), “Model updating for Nam O bridge using particle swarm optimization algorithm and genetic algorithm”, *Sensors*, **18**(12), 4131. https://doi.org/10.3390/s18124131.

Vu-Bac, N., Lahmer, T., Zhuang, X., Nguyen-Thoi, T. and Rabczuk, T. (2016), “A software framework for probabilistic sensitivity analysis for computationally expensive models”, *Adv. Eng. Softw.*, **100**, 19-31. https://doi.org/10.1016/j.advengsoft.2016.06.005

Wan, H.P. and Wei-Xin, R. (2015), “Parameter selection in finite-element-model updating by global sensitivity analysis using Gaussian process metamodel”, *J. Struct. Eng.*, **141**(6), 04014164. https://doi.org/10.1061/(ASCE)ST.1943-541X.0001108.

HJ